Eurographics Workshop on Visual Computing for Biology and Medicine (2021)
S. Oeltze-Jafra, N. N. Smit, and B. Sommer (Editors)

2.5D Geometric Mapping of Aortic Blood Flow Data for Cohort Visualization

B. Behrendt[1], D. Pleuss-Engelhardt[1], M. Gutberlet[2] and B. Preim[1]

[1]Dept. of Simulation and Graphics, University of Magdeburg, Germany
[2]Dept. of Diagnostic and Interventional Radiology, Herzzentrum Leipzig, Germany

Abstract

*Four-dimensional phase-contrast magnetic resonance imaging (*4D PC-MRI*) allows for a non-invasive acquisition of time-resolved blood flow measurements, providing a valuable aid to clinicians and researchers seeking a better understanding of the interrelation between pathologies of the cardiovascular system and changes in blood flow patterns. Such research requires extensive analysis and comparison of blood flow data within and between different patient cohorts representing different age groups, genders and pathologies. However, a direct comparison between large numbers of datasets is not feasible due to the complexity of the data.*

In this paper, we present a novel approach to normalize aortic 4D PC-MRI datasets to enable qualitative and quantitative comparisons. We define normalized coordinate systems for the vessel surface as well as the intravascular volume, allowing for the computation of quantitative measures between datasets for both hemodynamic surface parameters as well as flow or pressure fields. To support the understanding of the geometric deformations involved in this process, individual transformations can not only be toggled on or off, but smoothly transitioned between anatomically faithful and fully abstracted states. In an informal interview with an expert radiologist, we confirm the usefulness of our technique. We also report on initial findings from exploring a database of 138 datasets consisting of both patient and healthy volunteers.

CCS Concepts

• ***Human-centered computing*** → ***Visualization toolkits;*** *Information visualization;*

1. Introduction

Numerous cardiovascular pathologies, such as Marfan syndrome and bicuspid aortic valves (*BAV*), have been related to both changes in vascular morphology as well as to specific blood flow patterns [vBB*10, BMB*12, MBS*14]. 4D PC-MRI allows for a non-invasive acquisition of vascular geometry as well as time-resolved blood flow measurements within a 3D volume. This is a valuable aid for clinicians and researchers seeking a better understanding of the causes and effects of these pathologies and can ultimately lead to improved treatment decisions. 4D PC-MRI can be applied to a variety of vascular structures, such as ventricles, and the pulmonary artery. This paper focusses on analyzing aortic blood flow.

A key part of gaining insights into these pathologies is the systematic comparison between cohorts. While a visual comparison of singular datasets, e.g. using side-by-side views, is possible, a systematic analysis of large cohorts is not feasible this way. Similarly, a direct comparison of hemodynamic parameters from multiple datasets is challenging due to the complexity of the data, high interpersonal variations in vascular morphology and differences in acquisition parameters, such as the exact location of the vessel within the data volume.

In this paper, we present an approach to enable clinical researchers to intuitively explore and compare a large number of aortic blood flow datasets. We employ the (freely available) *Bloodline* system (`https://github.com/BenKoehler/Bloodline`) [KGGP19] for the necessary preprocessing (segmentation, computation of pathlines and flow parameters, identification of anatomical landmarks).

Based on the datasets segmentations, morphological variations are parameterized and can be individually removed from the data. The transformation between a faithful representation of the data and the abstracted geometry are fully animated to support the understanding of the geometric transformations involved. In its abstracted state, the surface mesh of the vessel is invariant to the actual vessel geometry and therefore can be directly compared between different datasets with respect to its hemodynamic parameters such as pressure, wall shear stress (*WSS*) or oscillatory shear index (*OSI*). Medical researchers can apply logical operations to these hemodynamic parameter maps and combine them into *composite maps* over multiple datasets using statistical measures such as average or standard deviation. The resulting composite maps can then be visualized by projecting them onto both faithful and ab-

DOI: 10.2312/vcbm.20211348

stract representations of a dataset. A visual comparison of multiple composite maps is enabled by a side-by-side visualization.

2. Related Work

The visualization and comparison of structurally complex and highly variable data, such as the blood flow within the aorta, is challenging. Numerous techniques have been developed to reduce the visual complexity and make various aspects of these datasets comparable.

Comparative Flow Visualization. *Image-based* comparisons are based on output images of visualizations. Often, the data is abstracted to focus on its main characteristics and avoid visual clutter. Born et al. [BMGS13] fuse representative lines of pathline bundles into 3D arrows to convey their principle flow direction. Similarly, vortex structures are depicted as tubes, focussing on their position and size rather than individual lines.

Lamata et al. [LPK*14] introduce spatio-temporal pressure maps displaying the average pressure around a centerline point in relation to time steps and distance of the point from the mitral valve. The resulting images allow for an easy qualitative comparison between datasets. However, as the maps use the absolute distance from the mitral valve as their y axis, quantitative comparisons between patients with differences in size or shape of the aorta can be challenging. Karimkeshteh et al. [KKN*19] eliminate this issue by normalizing the aorta between a set of pre-defined landmarks. The pressure along the centerline is visualized as a line graph, allowing comparisons between and within larger cohorts.

Van Pelt et al. [vGL*14] map glyphs onto the surface of cerebral aneurysms to compare hemodynamic flow parameters of the vessel surface, such as wall shear stress, from simulations with different stent configurations of the same dataset. Köhler et al. automatically classify flow patterns within the aorta [KGP*13] and mark their spatial and temporal extent in a Bull's Eye Plot [KMP*15], supporting a qualitative comparison of multiple datasets. This approach was refined by Meuschke et al. [MKP*16] to track individual vortices over the spatio-temporal domain of the dataset. Behrendt et al. [BEGP18] use planar reformats at normalized cross-section positions to juxtapose aspects of the flow field of two 4D PC-MRI datasets. Additionally, *data-driven* comparison techniques are available to directly compare the underlying data. Similar to the approach by Köhler et al., averaged differences between the cross-sections of the two datasets for each time step and centerline point, such as flow velocity or angle, are mapped to a Bull's Eye Plot to allow for a quick localization of *potentially interesting* cross-sections.

Flattening. Due to the branching and tubular shape of vascular structures, surface regions inherently overlap. Thus, several techniques have been developed to unfold or flatten vascular structures in order to reduce or prevent overlaps [KMM*18]. Angelelli and Hauser [AH11] use the straightening of tubular flow structures such as the aorta to facilitate overviews and comparisons within a singular dataset. By juxtaposing the straightened structures, multiple representations of one dataset, e.g. different time points, camera angles or visualization parameters, can be shown at the same time. A comparison between different datasets, e.g. vessels from different patients or the same patient at different points in time, is not inherently supported. Zhu et al. [ZHT05] present two algorithms (one angle-preserving, one area-preserving) to flatten the surface of branching vascular structures. Marino and Kaufman [MK16] propose a general flattening technique for tree-like structures. The surface area of the structure is flattened and the skeleton is deformed in a way that prevents self-occlusion. Thus, the entire surface of the object is visible while retaining as much of the original shape of the structure as possible.

Curved planar reformation (*CPR*) are commonly used to provide an overview of vascular structures. For this purpose, vascular structures are *distorted*, for example based on their centerlines, into a less curved or even fully straight shape [KFW*02]. For a *projected CPR*, parallel projection alongside an axis perpendicular to the vessels main axis is used to project the volume data onto an image. In a *stretched CPR*, the main axis of the vessel is curved in one dimension, while remaining planar in the other [KFW*02]. Unlike with a projected CPR, a stretched CPR retains isometry of the vessel. A *straightened CPR* results in a fully straightened depiction of the vessel where all points on the centerline are colinear. This type of CPR retains isometry and is particularly well suited for spotting variances in vessel diameter, but may result in a loss of spatial orientation.

Ropinski et al. [RHR*09] facilitate comparability of aortic arches of mice by applying a straightened multipath CPR and flatten the vessel surface using ray casting from the centerline. The inclusion of branching vessels from the aorta provides orientation in the straightened visualization. Mistelbauer et al. [MMV*13] introduce Curvicircular Feature Aggregation (*CFA*), a technique to aggregate vessel features, such as stenoses or calcifications, along circular rays around the centerline into a single image and display them in a straightened fashion. Unlike CPR, CFA enables the examination of the vessel lumen without the need to rotate around the centerline. Similarly, Diepenbrock et al. [DHS*13] proposed *normalized circular projection* to compare PET and CT data of animal coronary arteries straightened in a single image.

3. Data Acquisition & Preprocessing

Our clinical datasets were acquired using 1.5T or 3T MRI-machines from Siemens Healthcare, producing three magnitude images representing flow speed and three directional images representing flow in x-, y- and z-direction, respectively. These datasets were imported, segmented and pre-processed using the *Bloodline* system [KGGP19]. We describe the importation process in this section.

In *Bloodline*, image artifacts, such as phase wraps and eddy current artifacts, are corrected first. Afterwards, a segmentation of the aorta is performed semi-automatically using interactive graph cuts [BJ01]. By iteratively specifying regions as belonging to the foreground or background, a binary segmentation is created, which in turn is converted to a surface mesh using the Marching Cubes algorithm with additional volume-preserving smoothing. A centerline is extracted using an intravascular vessel wall distance map, requiring the user to manually select a start and end point on the

vessel wall. All centerline points are distributed equidistantly and for each point, a local orthogonal coordinate system (*LCS*) is calculated. The *xy*-plane of the LCS corresponds to the cross-sectional plane, with the z axis following the tangent of the centerline at the current point. As described by Köhler et al. [KPG*16], the orientation of the *xy*-plane (i.e. its rotation around the z-axis) is ensured to be consistent. After the extraction of the centerline, six cross-sectional landmarks following the definition of Schulz-Menger et al. [SMBB*13] are manually added to the vessel. Lastly, pathlines are integrated using Runge-Kutta (*RK4*) integration from the imported flow images. All manual segmentation steps for our datasets were carried out by our collaborating radiologists.

Bloodline is capable of exporting all processed information (i.e. preprocessed image data, surface mesh, pathlines, landmarks and centerline) in a structured format, which is in turn imported into our application. During the import step, we manually annotate the data as depicting a specific pathology (Tetralogy of Fallot or BAV) or belonging to a healthy volunteer. In total, our database contains fully segmented datasets from 22 BAV patients, 10 Fallot patients and 106 healthy volunteers.

4. Method

The following section details both basic visualization details as well as each step from a faithful to a flattened representation of the vessel. Additionally, we describe the process of mapping hemodynamic surface parameters into an anatomy-invariant space to compute composite parameter maps over multiple datasets.

4.1. Basic Visualization Techniques

The vessel surface is visualized using a 3D surface model and illuminated using Phong Shading with a single headlight. Blood flow is represented by pathlines, drawn as a connected sequence of view-aligned quads. Field data is visualized using a dense grid of points (Fig. 1). Hemodynamic parameters such as pressure can be mapped onto surface, pathlines and grid points using a variety of color scales with configurable value ranges. Both explicit (discarding based on parameter value) and implicit filtering (mapping a parameter to opacity) are available for all types of geometry. The value range used for the mapping of a hemodynamic parameter is automatically determined initially using both the actual value range from the data D as well as the semantic of the parameter, but can be freely adjusted manually. For example, OSI is shown with a range of $[0, 0.5]$ by default, while pressure always uses $[-\max_{v \in D}|v|, \max_{v \in D}|v|]$ to ensure 0 is in the middle of the range.

Pathlines as well as some field parameters (such as pressure) are time-resolved and thus can be animated. When the animation is enabled, only pathline segments *belonging* to a rolling temporal window with user-defined length around the current animation time point are visible. Similarly, the value shown on grid points is linearly interpolated between the time step before and after the current time point. To prevent pathlines, grid points, and surfaces from overlapping each other, they can be individually toggled or rendered semi-transparently. Additionally, both front-face culling or a silhouette view can be enabled for the vessel surface. Overlaps of transparent objects in the visualization are resolved using order-independent transparency [Thi11].

The user can create additional views, displaying either multiple datasets or variations of the same dataset. The position and rotation of each dataset in world space is matched based on the vessel surface bounding box and the camera of each view is synchronized, ensuring all views display the same anatomical region of the datasets at all times. Interactions such as displaying a specific hemodynamic parameter using a color scale can be performed independently for each view or synchronized over all views. The value ranges for color scales are synchronized between the views by default, but can also be manually adjusted.

4.2. Centerline-Based Representation

The coordinates of surface, centerline and pathline points $\vec{p} = (x_p, y_p, z_p)$ are given in world coordinates, referring to a cartesian grid with the origin $\vec{o} = (0,0,0)$ (Fig. 2a). To enable fast and flexible flattening of the data, we transfer the surface and pathline points into *centerline space* (Alg. 1), where the position of each point is defined by its relative position to its closest centerline point. Therefore the straightening only has to be applied to the centerline points and will *automatically* reflect on surface and pathlines as well. The transformation to centerline space is facilitated by first transferring the coordinates $\vec{p}$ from the cartesian world coordinates into a local coordinate system $\vec{p_c} = (x_{p_c}, y_{p_c}, z_{p_c})$ originating from the closest centerline point c (Fig. 2b). If $\vec{p}$ has multiple closest centerline points, the point closest to the beginning of the centerline is chosen. x_{p_c} and y_{p_c} refer to the position of the projection of $\vec{p}$ onto the cross-sectional plane of c, while z_{p_c} encodes the distance from said plane. The closest centerline point c to $\vec{p}$ is efficiently determined using a *KD Tree*.

This representation is suitable for straightening and length normalization of the aorta, yet still does not allow for an easy flattening. Thus instead of expressing the position x_{p_c}, y_{p_c} of $\vec{p_c}$ on the centerline plane in cartesian coordinates we use polar coordinates $\vec{p_c} = (\alpha_{p_c}, r_{p_c}, z_{p_c})$, with α_{p_c} representing the angle and r_{p_c} representing the radius (Fig. 2c). Additionally, all components of the polar coordinate vector are individually normalized to a $[0,1]$ value range.

We employ a two-pass rendering approach using *Transform Feedback* to visualize the surface and pathline data with this format. For the first pass, we upload the centerline as an array of points together with the axes of their respective local coordinate system to the GPU. Each surface or pathline vertex is uploaded using the previously described local polar coordinates. Additionally, we store the index of the closest centerline point for each vertex. A combination of vertex and geometry shaders convert the polar coordinates back into cartesian coordinates and use the position and coordinate system of the associated centerline point to transfer them to the world coordinate system for the purpose of rendering. The resulting vertices are stored in an additional buffer and rendered within the second pass. This approach enables interactive deformation of the vessel in real-time.

Algorithm 1 Converting to centerline-based representation

```
1:  procedure toCenterlineRepresentation
2:      cl ← list of all n centerline points
3:      lcsX, lcsY, lcsZ ← local axes for all n centerline points
4:      verts ← list of all m pathline/surface vertices
5:
6:      ▷ Create transformation matrices into all CL point's LCS
7:      for i ← [1..n] do
8:          transform[i] ← mat4( colums(lcsX[i], lcsY[i], lcsZ[i]) )
9:
10:         ▷ Transform each vertex into LCS of closest CL point
11:     maxWidth ← 0
12:     for i ← [1..m] do
13:         c ← indexOf( kdClosest( verts[i], cl ) )
14:         verts[i] ← transform[c] × (verts[i] − cl[c])
15:         verts[i].xy ← toRadial(verts[i].xy)
16:         maxWidth ← max(verts[i].y, maxWidth)
17:
18:                 ▷ Normalize LCS coordinates of each vertex
19:     for i ← [1..m] do
20:         c ← indexOf( kdClosest( verts[i], cl ) )
21:         verts[i].x ← verts[i].x/PI × 2
22:         verts[i].y ← verts[i].y/maxWidth
23:         verts[i].z ← verts[i].z/distance(cl[c], cl[c+1])
```

4.3. Length and Width Normalization

As mentioned before, the surface and pathline geometry is expressed relative to the centerline. To perform the straightening, we determine the angle between each line segment of the centerline. Based on the user-defined straightening factor $f_s \in [0,1]$, this angle is interpolated between its original value and 180°, resulting in a smooth straightening animation when transitioning f_s from 0 to 1 (Fig. 3a). Additionally, we move the dataset in its entirety to keep it centered after the straightening.

The centerline is segmented into seven sections by the six landmarks imported from *Bloodline*, namely the aortic valve, mid-ascending aorta, directly before the brachiocephalic trunk, in between the left common carotid and left subclavian artery, behind the left subclavian artery and in the mid-descending aorta [KGGP19]. As our collaborating physicians are familiar with viewing 4D PC-MRI datasets in *Bloodline*, we use the same coloring (Fig. 3b) for the landmarks on the centerline.

To facilitate an abstract visualization of the aorta, we stretch or compress each segment to an equal length (Fig. 3b, bottom). Similar to the straightening process, we employ a user-defined length normalization factor $f_l \in [0,1]$ to interpolate between the original and normalized length of each segment, resulting in a smooth transition between both states. A side effect of the normalization is increased emphasis on the ascending aorta and aortic arch, which are usually stretched, as well as a deemphasis of the descending aorta, which is usually compressed. The first segment of the centerline before the aortic valve is ignored for the length normalization, as it does not actually belong to the aorta.

In addition to equalizing the length of the sections, it is also possible to remove local differences in vessel width and transform the vessel into a tube. A width normalization factor $f_w \in [0,1]$ controls the interpolation between the actual r_{p_c} component of each surface vertex' position in centerline space and the value 1, effectively moving all surface vertices to the same distance from the centerline (Fig. 3c). However, this same transformation can not be applied to the pathlines, as it would move all pathline vertices outwards from the vessel lumen push them fully *into* the wall. Instead, the r_{p_c} component of the pathline vertices must be transformed according to the local width of the vessel. To represent this information on the GPU, we resample the vessel surface in centerline space to a texture, with α_{p_c} and z_{p_c} being mapped to the xy- coordinates of the texture, and r_{p_c} as the value of each texel. Since the vertices of the vessel are not positioned in a regular grid, bilinear interpolation is not possible. Instead, the resampling is performed by identifying the four closest surface vertices in centerline space for each texel using a KD Tree, and interpolating their r_{p_c} value using Shepard interpolation. The resulting texture is then used by the GPU to look up the vessel width *above* each pathline vertex, and apply the scal-

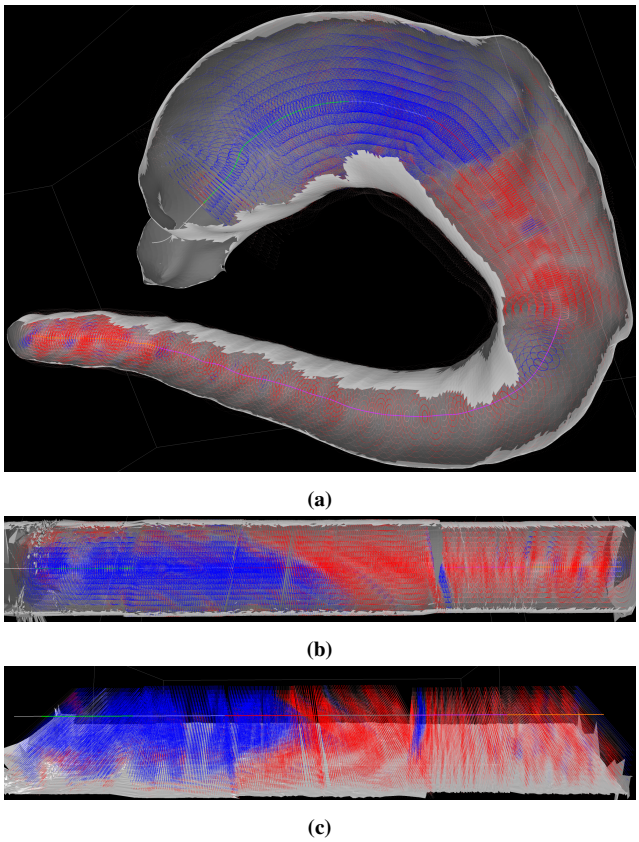

Figure 1: *Point-based field visualization with a faithful vessel representation (a), straightened and normalized in length and width (b) and flattened (c). In all cases, the intravascular pressure is mapped using a divergent red-transparent-blue scale. While the grid appears regular in the flattened representation, the actual sampling is performed circularly around the centerline, similar to Mistelbauer et al. and Diepenbrock et al. [MMV*13, DHS*13].*

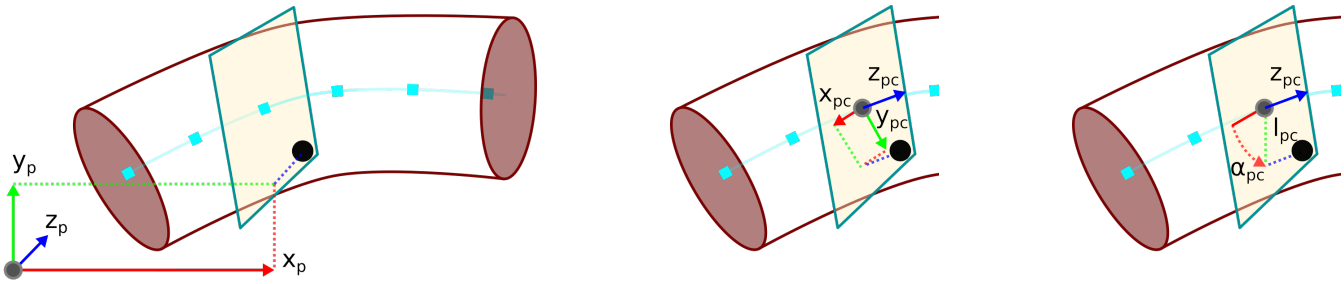

(a) (b) (c)

Figure 2: *Representation of a single point p within the vessel in world coordinates (a) as well as the cartesian (b) and polar (c) coordinate system of the cross-sectional plane belonging to its closes centerline point c.*

ing of the r_{p_c} component accordingly. We empirically determined a texture resolution of 1024×1024 to be sufficiently detailed while remaining computationally feasible for this process.

4.4. Flattening

To flatten the vessel surface and pathlines, we map the α_{p_c} and z_{p_c}- components of their vertex position in centerline space directly onto the *yz*- plane of each centerline point's local coordinate system. Once again, a smooth transition between the flattened and non-flattened state is facilitated by a flattening factor $f_f \in [0,1]$ (Fig. 4). The interpolation effect mimics *cutting* the aorta open with a straight cut using a *knife* and then flattening its surface onto a table. Pathline segments and mesh faces intersecting the virtual knife are disconnected once the interpolation factor is set to any value above 0. The result of this transformation for the vessel surface is a 2.5D *ribbon* moving alongside the centerline with pathlines or grid points hovering above (Fig. 4b). If f_w is not set to 1 to normalize the vessel width, the ribbon will show *bumps* reflecting local differences in vessel thickness (Fig. 5).

f_l, f_w, f_s and f_f can be controlled individually, thus allowing to independently toggle the different aspects of our transformation. With all four be set to 1, the surface mesh is transformed into a flat plane, with the grid points and pathlines positioned above, creating a 2.5D representation of the vessel wall and blood flow (Fig. 1c and 4).

4.5. Focus Region Selection

Users have the option to select a focus region within all views by dragging the cursor over the vessel surface and drawing a selection rectangle. The focus region is synchronized between all views. Once a focus region is selected, only pathlines *within* this region are drawn. Additionally, outside of the focus region the saturation of the vessel surface is strongly reduced. Figure 6 shows a comparison of a region in the ascending aorta between a patient with a BAV (top) and a healthy volunteer (bottom). The visualization not only highlights the difference in flow velocity, but also direction. The flat representation (Fig. 6a) clearly shows larger amounts of flow in axial direction, indicating the presence of a vortex, which can easily be missed the faithful representation (Fig. 6b).

4.6. Surface Parameter Mapping

Each surface vertex can be mapped onto a texture position using its normalized polar LCS coordinates $\alpha_{p_c}, l_{p_c} \in [0,1]$ (Fig. 7). This enables the rendering of their associated hemodynamic parameters, such as WSS or OSI, to be drawn into a texture invariant to morphological properties of individual aorta shapes. These textures can then not only be mapped onto a different dataset, but compared directly on a per-pixel basis to compute averages or difference maps over multiple datasets. Whenever a dataset is loaded, such textures are automatically created for each hemodynamic surface parameter. Similar to the local vessel width map, texel values are calculated by Shepard interpolation from the four closest vertices. Once again, the first segment of the centerline before the aortic valve is ignored for this mapping. We determined a resolution of 360×720 to produce textures with sufficient detail to capture all hemodynamic features of the surface mesh while remaining computationally feasible. The horizontal resolution of 360 allows each degree of rotation around the centerline to be captured by a single pixel while the vertical resolution of 720 ensures a spatial resolution of *1mm* along the centerline even in the strongly compressed sections of the descending aorta.

We include an editor allowing users to create basic mathematical functions to calculate new *composite* textures from existing parameter images over multiple datasets. The available functions are *min*, *max*, *average* and *standard deviation*. Users may normalize the value range of each individual parameter image before applying these functions. Figure 8 shows a composite texture of the lowest and highest OSI values over all volunteer (Fig. 8a) and BAV patient datasets (Fig. 8b) mapped to the vessel model of a volunteer. Interestingly, the highest OSI values for BAV patients do not seem to systematically exceed those of the volunteer datasets, with the volunteer datasets even containing higher OSI values in some places compared to the BAV datasets. On the other hand, the lowest OSI values of BAV patients seem to be generally higher, especially in the aortic arch.

5. Evaluation

To evaluate our approach, we examine its computational complexity and conduct an interview with a medical expert. Additionally,

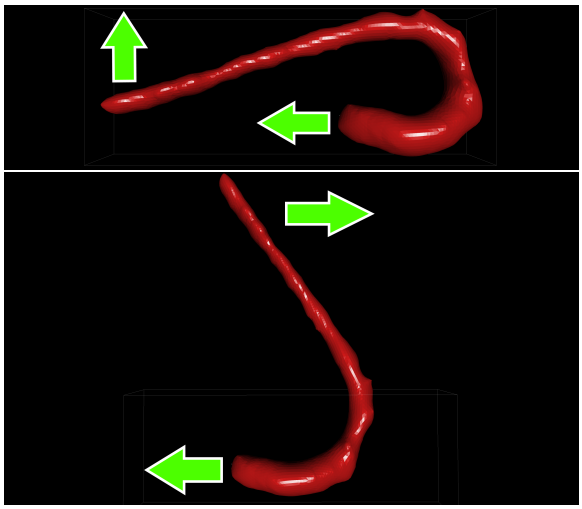

(a) *Vessel straightening. Arrows indicate movement direction.*

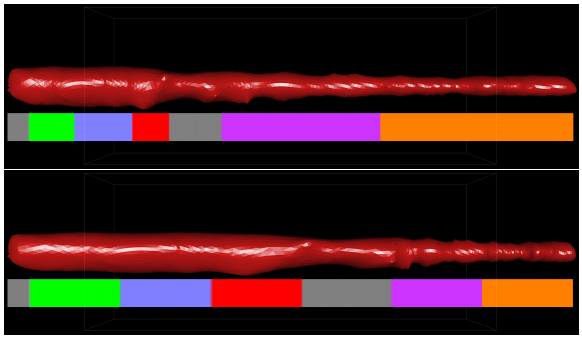

(b) *Length normalization with overlaid centerline sections*

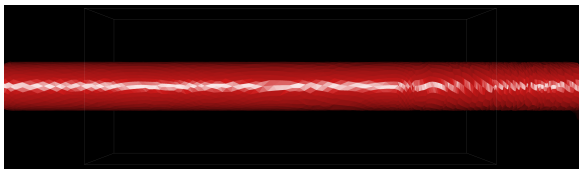

(c) *Normalized tubular representation*

Figure 3: *Transformation of the aorta from a faithful representation onto a normalized tubular representation. The vessel is straightened (a), each section of the centerline is stretched or compressed to the same length (b) and the radius of all sections is increased to the largest vessel diameter in the dataset (c).*

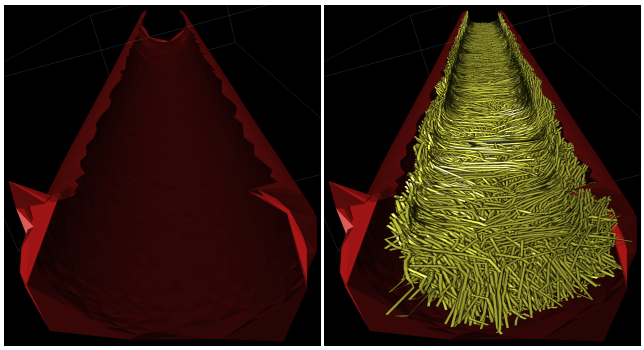

(a) Cutting *and flattening the vessel without (left) and with (right) pathlines*

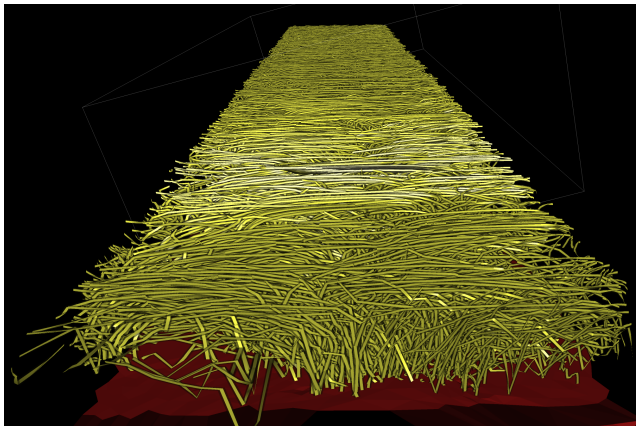

(b) *Result of the flattening with pathlines*

Figure 4: *Vessel flattening. The vessel is* cut open *(a) with the surface moving to the bottom and the pathlines hovering above (b).*

we report on some initial findings from exploring our database of 4D PC-MRI datasets.

Performance

The data visualization itself is fully interactive and not overly taxing for a modern GPU. Due to the representation of the data in centerline space, the geometric deformation only requires updating the centerline, which is performed on the CPU and does not cause any noticeable delay. Opening a dataset within our prototype for the first time requires the surface and pathlines to be transformed into centerline space. On an *AMD Ryzen 7 2700X* processor with 8 physical cores clocked at 4000MHz, this process takes roughly 35 seconds. Subsequent openings of the same dataset are significantly faster (2 seconds), as the transformation results are cached. When opening a dataset only for extracting a normalized hemodynamic surface parameter map several steps of the transformation are skipped (most importantly the transformation of all pathlines into centerline space), reducing the processing time to 3 seconds. Therefore, the system is able to process around 20 – 30 datasets a minute when calculating composite parameter maps.

Expert Interview

We conducted an informal interview with an expert radiologist (male, >20 years experience, co-author) and presented him our prototype via an online video conference system and screen sharing. We operated the graphical user interface according to the experts instruction, although at multiple points the expert took control over the application himself, mostly to operate the camera.

He described the 2.5D display of pathlines as especially useful for the classification of vortices. Vortices are often classed as *helical*, i.e. swirling in place without forward movement, or *vortical* when they do contain forward movement. In the 2.5D visualization,

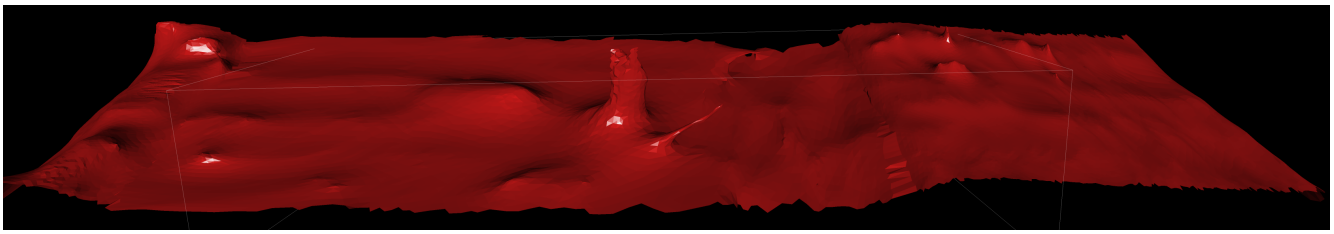

Figure 5: *Flattened representation without width normalization. Local differences in vessel radius as well as branching vessels are visible as bumps on the surface plane.*

vortices appear as pseudo-laminar flow lateral to the centerline, with exactly perpendicular flow representing *helical* flow. Thus, the expert found it easier to distinguish different types of vortices with the 2.5D visualization.

While the expert pointed out that the smooth animation as well as the ability to individually control all aspects of the flattening was helpful to understand the geometric transformations that are involved, he wished for an additional guidance system. In addition to displaying the centerline and color-encoding the specific sections of the aorta, he proposed overlaying a grid instead. This would not only provide additional guidance, but also allow for an easier description of the location of a feature (e.g. "ascending aorta, cell A1 - B3").

During the evaluation, the expert asked us to calculate the highest WSS magnitude values for BAV patients and healthy volunteers, which we once again mapped onto a proxy dataset from a healthy volunteer for the purpose of visualization (Fig. 9). As expected, the visualization clearly shows higher WSS in the aortic arch as well as the ascending aorta. However, the expert was surprised to see that increased WSS in the aortic arch can also appear within healthy volunteers. Overall, the expert described the generation of composite parameter maps as highly useful to determine standard values for hemodynamic parameters within various patient or volunteer cohorts.

6. Conclusion & Future Work

In this paper, we have presented a novel approach to facilitate comparability between hemodynamic parameters of 4D PC-MRI aortic blood flow datasets. Vessel surface and pathlines are transformed into a normalized *centerline space* and subsequently flattened into a 2.5D representation to reduce occlusion. The field and pathline visualizations provide context information about the time-resolved blood flow. Transitions between faithful and flattened representations of the data are smoothly animated to support the understanding of the geometric deformations involved. In the flattened state, the pathline visualization also allows for an easier distinction between vortical and helical flow.

Hemodynamic surface parameters can be directly compared and evaluated between arbitrary amounts of datasets to support an efficient analysis of cohorts. The resulting composite surface parameter maps can either be explored individually or compared visually in synchronized side-by-side views. We reported on some initial medical findings from our expert interview that could serve as starting points for further investigation. An integration of visual analysis techniques would enable a more thorough statistical analysis of cohorts. For example, selecting a point on the vessel surface with a composite map could bring up statistical graphs, such as histograms or box plots for this specific point over all datasets from the cohort. Additionally, more complex mapping techniques could be explored, such as displaying the parameter variance of a region within the cohort using glyphs.

For this paper, we have focussed on comparing surface features. However, time-dependent field data (such as pressure or the flow field itself) could also be transformed into normalized centerline space and used for quantitative comparisons. This poses additional challenges, as the resulting parameter textures would need to be four-dimensional (including the time and distance from the centerline as additional axes). Although all datasets represent a single heart beat, neither heart rate nor the exact alignment within the cardiac cycle is necessarily consistent between individual datasets. Therefore an additional temporal normalization would be required. Transforming the flow field into centerline space would not only allow seeding pathlines based on the transformed field, but also integrating pathlines from a composite field created from multiple datasets. These *composite pathlines* could lead to further insights on fundamental similarities between cohorts, such as vortices that appear in a significant number of individual datasets for a specific group.

Especially in a medical context, changing the size or shape of objects can be problematic if this change is not properly conveyed to the viewer. Although the ability to transition between the different stages of flattening alleviates this issue to a degree, additional visual cues could be added to mark regions with particularly high levels of deformation. For example, high differences in surface area or angles between faithful and flattened state could be encoded on the faces of the vascular mesh using hatching.

Flattened visualizations exhibit distortions: Distances and angles cannot be perfectly preserved. From a practical point of view, the amount of these distortions is probably less interesting since for a physician it is clear that the visualizations created here, like many CPR variants used in clinical routine, are strongly simplified abstractions. They provide an overview and may indicate whether a certain pattern exist for the patient. For any in-depth information on the location of a pattern, physicians check with data that is not reformatted, such as original data.

Our approach does not support branching centerlines and is tailored towards the aorta, as it incorporates specific landmarks. While

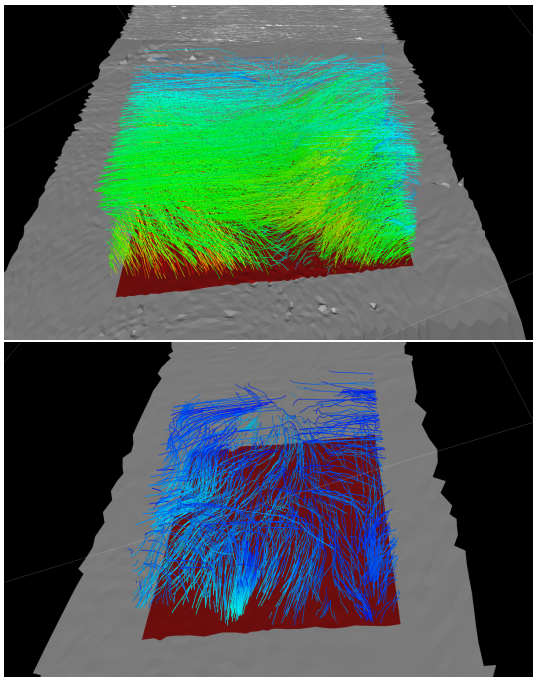

(a)

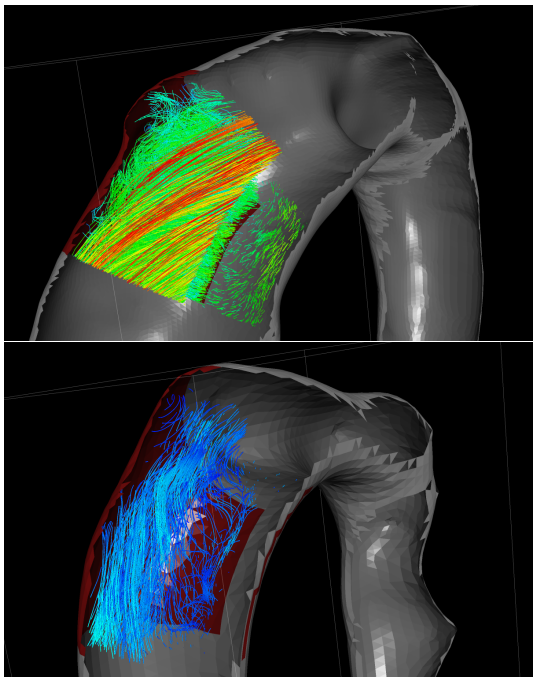

(b)

Figure 6: *Comparison of a focus region within the ascending aorta between two datasets in flattened (a) and faithful (b) representation. Pathlines are color-coded with a rainbow scale based on the flow velocity. The rainbow scale was chosen as it allows the perception of smaller differences despite a comparatively large total value range.*

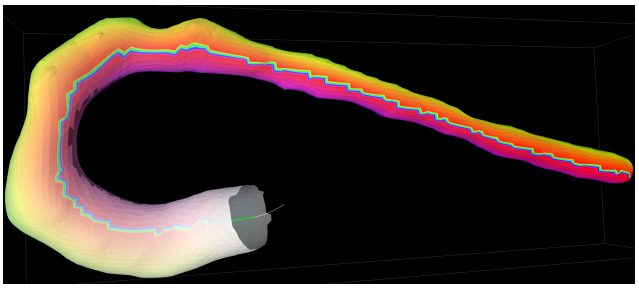

(a)

(b)

Figure 7: *Association between vessel surface and surface parameter texture position using hue and saturation on a faithful (a) and flattened (b) vessel representation. For the faithful representation, the cutting line is also visible.*

adjustments to support a different set of landmarks can be easily made, e.g. to apply our prototype to the thoracic aorta, support for branching vessels such as the pulmonary artery would require several reworks for the normalization process. Additional challenges would arise for vascular structures such as the *Circle of Willis* that have a circular structure and a high inter-personal variance with regard to the size and existence of certain branches.

Acknowledgements

We would like to thank *Gabriel Mistelbauer* for his valuable feedback, both in regards to our prototype as well as for his suggestions for improvements on this paper.

References

[AH11] ANGELELLI P., HAUSER H.: Straightening tubular flow for side-by-side visualization. *IEEE transactions on visualization and computer graphics 17*, 12 (2011), 2063–2070. doi:10.1109/TVCG.2011.235. 2

[BEGP18] BEHRENDT B., EBEL S., GUTBERLET M., PREIM B.: A framework for visual comparison of 4D PC-MRI aortic blood flow data. In *Eurographics Workshop on Visual Computing for Biology and Medicine* (2018). doi:10.2312/vcbm.20181236. 2

[BJ01] BOYKOV Y. Y., JOLLY M.-P.: Interactive graph cuts for optimal boundary & region segmentation of objects in n-d images. In *Eighth IEEE International Conference on Computer Vision* (2001), pp. 105–112. doi:10.1109/ICCV.2001.937505. 2

[BMB*12] BARKER A. J., MARKL M., BÜRK J., LORENZ R., BOCK J., BAUER S., SCHULZ-MENGER J., VON KNOBELSDORFF-BRENKENHOFF F.: Bicuspid aortic valve is associated with altered wall shear stress in the ascending aorta. *Circulation. Cardiovascular imaging 5*, 4 (2012), 457–466. doi:10.1161/CIRCIMAGING.112.973370. 1

[BMGS13] BORN S., MARKL M., GUTBERLET M., SCHEUERMANN G.: Illustrative visualization of cardiac and aortic blood flow from 4D

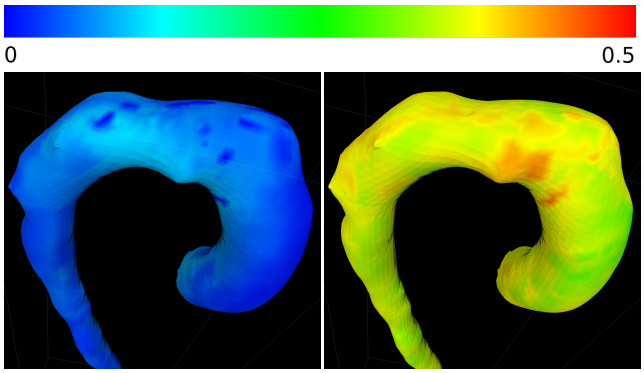

(a) *Lowest and highest OSI over all volunteer datasets*

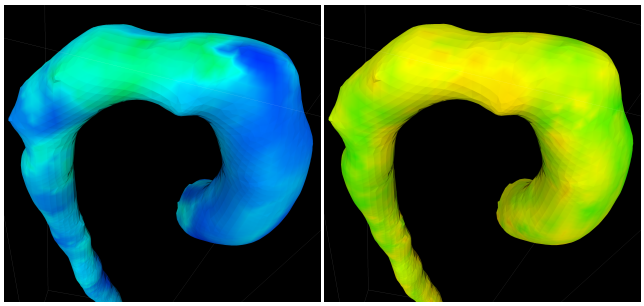

(b) *Lowest and highest OSI over all BAV datasets*

Figure 8: *Visual comparison of the lowest (left) and highest (right) OSI values over all healthy volunteers (Fig. a) and patients with BAV (Fig. b) mapped on a proxy dataset of a healthy volunteer using the rainbow scale.*

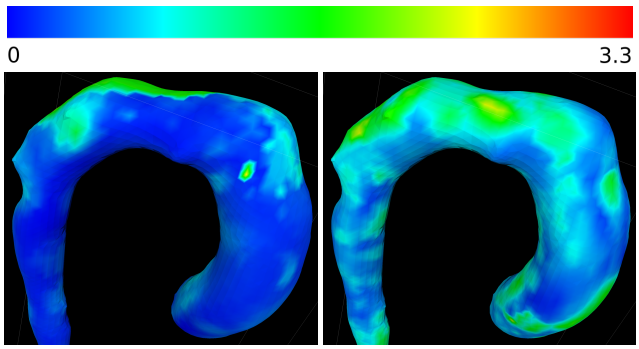

(a) **(b)**

Figure 9: *Visual comparison of the highest WSS magnitude values over all healthy volunteers (a) and patients with BAV (b) using the rainbow scale.*

MRI data. In *IEEE Pacific Visualization Symposium (PacificVis)* (2013), pp. 129–136. doi:10.1109/PacificVis.2013.6596137. 2

[DHS*13] DIEPENBROCK S., HERMANN S., SCHÄFERS M., KUHLMANN M., HINRICHS K.: Comparative visualization of tracer uptake in in vivo small animal PET/CT imaging of the carotid arteries. *Computer Graphics Forum 32*, 3pt2 (2013), 241–250. doi:10.1111/cgf.12111. 2, 4

[KFW*02] KANITSAR A., FLEISCHMANN D., WEGENKITTL R., FELKEL P., GRÖLLER E.: CPR - curved planar reformation. In *IEEE Visualization* (2002), pp. 37–44. doi:10.1109/VISUAL.2002.1183754. 2

[KGGP19] KÖHLER B., GROTHOFF M., GUTBERLET M., PREIM B.: Bloodline: A system for the guided analysis of cardiac 4D PC-MRI data. *Computers & Graphics 82* (2019), 32–43. doi:10.1016/j.cag.2019.05.004. 1, 2, 4

[KGP*13] KÖHLER B., GASTEIGER R., PREIM U., THEISEL H., GUTBERLET M., PREIM B.: Semi-automatic vortex extraction in 4D PC-MRI cardiac blood flow data using line predicates. *IEEE transactions on visualization and computer graphics 19*, 12 (2013), 2773–2782. doi:10.1109/TVCG.2013.189. 2

[KKN*19] KARIMKESHTEH S., KAUFHOLD L., NORDMEYER S., JARMATZ L., HARLOFF A., HENNEMUTH A.: Comparing subjects with reference populations - a visualization toolkit for the analysis of aortic anatomy and pressure distribution. In *Functional Imaging and Modeling of the Heart*, vol. 11504 of *Lecture Notes in Computer Science*. Springer International Publishing, 2019, pp. 370–378. doi:10.1007/978-3-030-21949-9_40. 2

[KMM*18] KREISER J., MEUSCHKE M., MISTELBAUER G., PREIM B., ROPINSKI T.: A survey of flattening-based medical visualization techniques. *Computer Graphics Forum 37*, 3 (2018), 597–624. doi:10.1111/cgf.13445. 2

[KMP*15] KÖHLER B., MEUSCHKE M., PREIM U., FISCHBACH K., GUTBERLET M., PREIM B.: 2d plot visualization of aortic vortex flow in cardiac 4D PC-MRI data. In *Bildverarbeitung für die Medizin 2015*. 2015, pp. 257–262. doi:10.1007/978-3-662-46224-9_45. 2

[KPG*16] KÖHLER B., PREIM U., GROTHOFF M., GUTBERLET M., FISCHBACH K., PREIM B.: Robust cardiac function assessment in 4D PC-MRI data of the aorta and pulmonary artery. *Computer Graphics Forum 35*, 1 (2016), 32–43. doi:10.1111/cgf.12669. 3

[LPK*14] LAMATA P., PITCHER A., KRITTIAN S., NORDSLETTEN D., BISSELL M. M., CASSAR T., BARKER A. J., MARKL M., NEUBAUER S., SMITH N. P.: Aortic relative pressure components derived from four-dimensional flow cardiovascular magnetic resonance. *Magnetic resonance in medicine 72*, 4 (2014), 1162–1169. doi:10.1002/mrm.25015. 2

[MBS*14] MAHADEVIA R., BARKER A. J., SCHNELL S., ENTEZARI P., KANSAL P., FEDAK P. W. M., MALAISRIE S. C., MCCARTHY P., COLLINS J., CARR J., MARKL M.: Bicuspid aortic cusp fusion morphology alters aortic three-dimensional outflow patterns, wall shear stress, and expression of aortopathy. *Circulation 129*, 6 (2014), 673–682. doi:10.1161/CIRCULATIONAHA.113.003026. 1

[MK16] MARINO J., KAUFMAN A.: Planar visualization of treelike structures. *IEEE transactions on visualization and computer graphics 22*, 1 (2016), 906–915. doi:10.1109/TVCG.2015.2467413. 2

[MKP*16] MEUSCHKE M., KÖHLER B., PREIM U., PREIM B., LAWONN K.: Semi-automatic vortex flow classification in 4D PC-MRI data of the aorta. *Computer Graphics Forum 35*, 3 (2016), 351–360. doi:10.1111/cgf.12911. 2

[MMV*13] MISTELBAUER G., MORAR A., VARCHOLA A., SCHERNTHANER R., BACLIJA I., KÖCHL A., KANITSAR A., BRUCKNER S., GRÖLLER E.: Vessel visualization using curvicircular feature aggregation. *Computer Graphics Forum 32*, 3pt2 (2013), 231–240. doi:10.1111/cgf.12110. 2, 4

[RHR*09] ROPINSKI T., HERMANN S., REICH R., SCHÄFERS M., HINRICHS K.: Multimodal vessel visualization of mouse aorta PET/CT scans. *IEEE transactions on visualization and computer graphics 15*, 6 (2009), 1515–1522. doi:10.1109/TVCG.2009.169. 2

[SMBB*13] SCHULZ-MENGER J., BLUEMKE D. A., BREMERICH J., FLAMM S. D., FOGEL M. A., FRIEDRICH M. G., KIM R. J., VON KNOBELSDORFF-BRENKENHOFF F., KRAMER C. M., PENNELL D. J., PLEIN S., NAGEL E.: Standardized image interpretation and post processing in cardiovascular magnetic resonance: Society for cardiovascular magnetic resonance (scmr) board of trustees task force on standard-

ized post processing. *Journal of Cardiovascular Magnetic Resonance 15* (2013), 35. doi:10.1186/1532-429X-15-35. 3

[Thi11] THIBIEROZ N.: Order-independent transparency using per-pixel linked lists. *GPU Pro 2* (2011), 409–431. 3

[vBB*10] VAN PELT R., BESCÓS J. O., BREEUWER M., CLOUGH R. E., GRÖLLER M. E., TER HAAR ROMENIJ B., VILANOVA A.: Exploration of 4D MRI blood flow using stylistic visualization. *IEEE transactions on visualization and computer graphics 16*, 6 (2010), 1339–1347. doi:10.1109/TVCG.2010.153. 1

[vGL*14] VAN PELT R., GASTEIGER R., LAWONN K., MEUSCHKE M., PREIM B.: Comparative blood flow visualization for cerebral aneurysm treatment assessment. *Computer Graphics Forum 33*, 3 (2014), 131–140. doi:10.1111/cgf.12369. 2

[ZHT05] ZHU L., HAKER S., TANNENBAUM A.: Flattening maps for the visualization of multibranched vessels. *IEEE transactions on medical imaging 24*, 2 (2005), 191–198. doi:10.1109/TMI.2004.839368. 2